Biomech Model Mechanobiol
DOI 10.1007/s10237-014-0577-5

ORIGINAL PAPER

A computational model for cell/ECM growth on 3D surfaces using the level set method: a bone tissue engineering case study

Y. Guyot · I. Papantoniou · Y. C. Chai · S. Van Bael · J. Schrooten · L. Geris

Received: 10 December 2013 / Accepted: 19 March 2014

Abstract Three-dimensional open porous scaffolds are commonly used in tissue engineering (TE) applications to provide an initial template for cell attachment and subsequent cell growth and construct development. The macroscopic geometry of the scaffold is key in determining the kinetics of cell growth and thus in vitro 'tissue' formation. In this study, we developed a computational framework based on the level set methodology to predict curvature-dependent growth of the cell/extracellular matrix domain within TE constructs. Scaffolds with various geometries (hexagonal, square, triangular) and pore sizes (500 and 1,000 μm) were produced in-house by additive manufacturing, seeded with human periosteum-derived cells and cultured under static conditions for 14 days. Using the projected tissue area as an output measure, the comparison between the experimental and the numerical results demonstrated a good qualitative and quantitative behavior of the framework. The model in its current form is able to provide important spatio-temporal information on final shape and speed of pore-filling of tissue-engineered constructs by cells and extracellular matrix during static culture.

Keywords Level set method · Curvature based growth · Tissue engineering · Scaffold design

Y. Guyot (✉) · I. Papantoniou · Y. C. Chai · S. Van Bael · J. Schrooten · L. Geris
Prometheus, Division of Skeletal Tissue Engineering, KU Leuven, Onderwijs en Navorsing 1 (+8), Herestraat 49, PB 813, 3000 Leuven, Belgium
e-mail: yguyot@ulg.ac.be

Y. Guyot · L. Geris
Biomechanics Research Unit, Université de Liège, Chemin des Chevreuils 1, BAT 52/3, 4000 Liège, Belgium

I. Papantoniou · Y. C. Chai
Skeletal Biology and Engineering Research Center, KU Leuven, Onderwijs en Navorsing 1 (+8), Herestraat 49, PB 813, 3000 Leuven, Belgium

J. Schrooten
Department of Metallurgy and Materials Engineering, KU Leuven, Kasteelpark Arenberg 44, PB 2450, 3001 Leuven, Belgium

L. Geris
Biomechanics Section, Department of Mechanical Engineering, KU Leuven, Celestijnenlaan 300C, PB 2419, 3001 Leuven, Belgium
e-mail: liesbet.geris@ulg.ac.be

S. Van Bael
Division of Production Engineering, Machine Design and Automation, Department of Mechanical Engineering, KU Leuven, Celestijnenlaan 300b, 3001 Leuven, Belgium

1 Introduction

Three-dimensional (3D) porous scaffolds are commonly used in tissue engineering (TE) applications to provide an initial template for subsequent cell growth and construct development. Their architectural features, alongside with physicochemical characteristics, have been seen to play a significant role in important biological processes such as initial cell attachment (Melchels et al. 2010, 2011), cell growth, and extracellular matrix (ECM) formation during 3D in vitro culture (Zeltinger et al. 2001a; Hollister et al. 2002; Bael et al. 2012b). Geometrical scaffold properties such as pore size (Zeltinger et al. 2001b) and pore shape (Knychala et al. 2013), and more specific features such as curvature (Rumpler et al. 2008; Gamsjager et al. 2013) have been shown to constitute crucial design considerations in controlling cell fate both for in vitro (Rumpler et al. 2008) and in vivo applications (Bidan et al. 2012). Nelson et al. (2005) studied the hypothesis that scaffold geometry controls the evolving multicellular

Published online: 03 April 2014

construct geometry by defining patterns of mechanical stress throughout the structure, thereby enhancing cell proliferation. Furthermore, cell growth rate has been suggested to be dependent on mechanical stress, with a dependence of the rate of cell division on local stress regimes (Shraiman 2005; Dunlop et al. 2010) [For review on mechanotransduction see (Eyckmans et al. 2011)].

Literature on the numerical exploration of growth kinetics of cell/tissue structures driven by the geometric properties of scaffolds (Rumpler et al. 2008; Bidan et al. 2012; Gamsjager et al. 2013; Knychala et al. 2013) is expanding rapidly. The concept of curvature-controlled growth has been put forward by Dunlop et al. (13) to capture the previously mentioned dependence of cell growth kinetics on the local surface curvature of the substrate. Rumpler et al. developed a 2D model capable of capturing in vitro curvature-driven cell growth by advecting the cell/ECM surface with a curvature-dependent velocity. They recently extended their model to 3D, based on an analytical computation of the curvature which depends on a sphere (mask) browsing digital image-sets of the geometries of interest and compute the curvature within the mask (Bidan et al. 2013b). A major limitation of the aforementioned approach is its focus in symmetric 3D pore channel structures which cannot be extrapolated to complex and non-symmetrical scaffold geometries. Therefore, developing a model of curvature-dependent growth that readily and accurately allows simulation of cell/ECM growth over realistic convex or non-convex 3D scaffold geometries is important for the design of optimal TE scaffolds.

The development of additive manufacturing techniques has enabled the production of porous structures with controlled architectures suitable for TE applications (Bael et al. 2011; Sobral et al. 2011). However, their design characteristics still lack features to guide cell fate. Studies regarding cell–material interactions often focus on surface topography, microenvironment niches, and single-cell observations [for review see Higuchi et al. (2013), Lutolf and Hubbell (2005)] with limited translational relevance to TE. Currently, a wide variety of regular and irregular 3D scaffolds is reported in the literature, however, regular pore geometry scaffolds seem to offer certain advantages by minimizing intra-scaffold variability. In this work as a case study, 3D regular pore geometry Ti6Al4V (Ti) scaffolds were used, which in combination with human periosteum-derived cells (hPDCs) allow cell proliferation and differentiation to osteogenic phenotypes resulting in 3D mineralized constructs (Chai et al. 2012; Papantoniou et al. 2013b). Furthermore, when implanted ectopically in vivo, they have been shown to successfully induce bone formation (Chai et al. 2012a), thus constituting a promising system for further study.

A crucial parameter for robust TE process design will be the development of 'realistic' computational models that will be able to predict the behavior of such complex cell-scaffold systems under a range of culture process conditions. Expanding on the conclusions of the aforementioned experimental studies (Papantoniou et al. 2013b), we developed a 3D in silico model based on the level set method (presented in the next section). The aim of this paper is not to explore the mechanisms of curvature-dependent growth but rather to explore the use of the concept in a TE context by developing a computational framework capable of capturing the curvature-dependent cell/ECM growth and applying it to a range of 3D geometries.

2 Materials and methods

2.1 The level set method

In order to accurately simulate time-dependent events taking place in the cell/ECM component on the one hand and the remaining void space on the other, the level set (LS) method was used in this study (Sethian 1999). The LS method is a numerical method mainly used in multiphasic fluid dynamics (AlMomani et al. 2008) or image processing (Machacek and Danuser 2006) and phase transformations in metal physics applications (Javierre et al. 2006) to follow an interface between two moving domains. This method has also been used to model 2D growth kinetics of biological systems such as tumors (Hogea et al. 2006) and soft tissues (Lappa 2003a, 2005).

An important advantage of the LS technique in the context of this study is its intrinsic way of computing the mean curvature. Indeed the curvature only depends on the level set function ϕ and the mesh size; hence, it can be computed with minimal user intervention. The only element that the user has to provide is a meshed domain of the scaffold pore.

Define a domain $\Omega \subset \mathbb{R}^d$, $d = 2, 3$; and a decomposition of two subdomains Ω_1 and Ω_2 (where Ω_1 is the cell/ECM area/volume and Ω_2 the void area/volume) with the interface between them denoted as Γ and $\mathbf{n}$ the normal to this interface. The role of the LS method is to track implicitly the interface $\Gamma(t)$ moving with a velocity $\boldsymbol{u}$. The main objective of this method is a continuous scalar function φ defined on the domain. This level set function φ is a signed distance function chosen to be positive in Ω_1, negative in Ω_2, and zero on Γ. The interface tracking is described by an advection equation (1) of the level set function φ on the whole domain Ω. Equation (1) describes the Neumann (zero-flux) boundary condition.

$$\frac{\partial \varphi}{\partial t} + \boldsymbol{u} \cdot \nabla \varphi = 0 \quad \text{in} \quad \Omega \tag{1}$$

$$\nabla \varphi \cdot \boldsymbol{n} = 0 \quad \text{on} \quad \partial\Omega \tag{2}$$

The interface advection velocity $\boldsymbol{u}$ is determined in a similar manner to that reported in other curvature-controlled models

(Rumpler et al. 2008). In Rumpler et al. (2008), the authors describe that the cell/ECM interface moves faster where its local curvature κ is higher. Therefore, in this study, we define $\boldsymbol{u}$ as follows (see Fig. 1):

$$\boldsymbol{u} = \begin{cases} -\kappa \boldsymbol{n} & \textit{if } \kappa > 0 \\ 0 & \textit{if } \kappa \leq 0 \end{cases} \tag{3}$$

In this study, by using the LS method, the cell/ECM interface growth direction will be always from the surface of the strut toward the void pore ($\varphi < 0$) space as observed experimentally (Papantoniou et al. 2013b; Van Bael et al. 2012). This is the reason why Eq. (3) has a negative sign, indeed, according to our definition, the normal points toward the cell/ECM, so the growth velocity has to be directed along the opposite of the gradient of φ. As previously stated, the curvature of the interface as well as its normal is intrinsically computed with respect to the level set function φ, and their expression is as follows:

$$\boldsymbol{n} = \frac{\nabla \varphi}{|\nabla \varphi|} \tag{4}$$

$$\kappa = \nabla \cdot \boldsymbol{n}. \tag{5}$$

The curvature calculated in Eq. (4) corresponds to the mean curvature, similar to what was used by Bidan et al. (2013a,b).

2.2 Implementation

The full model was implemented using the finite element method (FEM) with an open source partial differential equation solver FreeFem++ (http://freefem.org) (Hecht 2012). This solver is well adapted for the type of model developed in this study due to its ability to deal with complex geometries and meshes, and its simplified way to treat any type of partial differential equation (PDE) by implementing its variational form. As a first step, relevant geometries were created with the (free) software SALOME (http://www.salome-platform.org) and then for the purpose of compatibility with FreeFem++, these geometries were meshed in a open source meshing software GMSH (geuz.org/gmsh/). A convergence study was executed to determine the optimal mesh size which in this study was taken to have around one million tetrahedrons for one pore.

To initialize the LS method, an initial distance function, φ_0, was defined in the domain Ω at the boundaries corresponding to the scaffold struts. Due to the very nature of distance functions, the level set function φ is not differentiable at certain locations (i.e., where gradient discontinuities may be found), thus the normal $\boldsymbol{n}$ and the curvature κ are not properly defined everywhere in the domain. In order to overcome this issue, an artificial diffusion term was added in the definition of $\boldsymbol{n}$ and κ (Eqs. (3) and (4)), leading to the equations shown in (4) and (6).

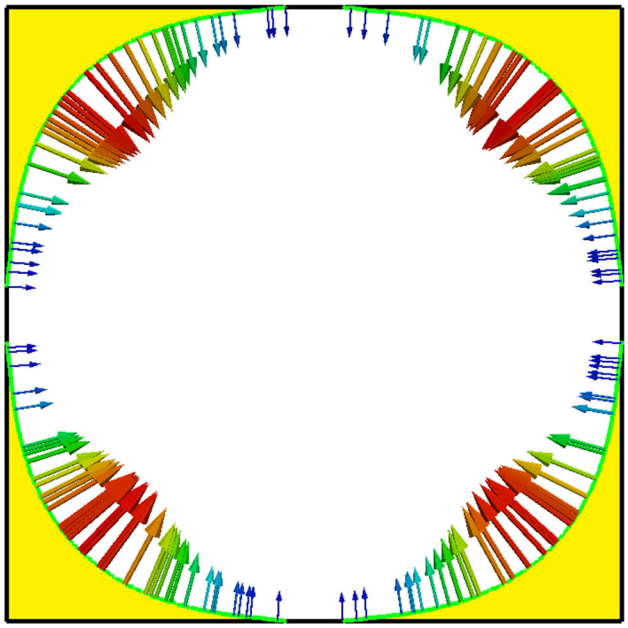

Fig. 1 Schematic representation of the level set approach. The cell/ECM interface ($\varphi = 0$) is represented in *green*, the cell/ECM domain ($\varphi > 0$) in *yellow*, and the 'empty' domain ($\varphi < 0$) in *white*. *Arrows* represent the curvature-controlled velocity, increasing from *blue* to *red*

$$\boldsymbol{n} = \frac{\nabla \varphi}{|\nabla \varphi|} + \varepsilon \Delta \boldsymbol{n} \tag{6}$$

$$\kappa = \nabla \cdot \boldsymbol{n} + \varepsilon \Delta \kappa \tag{7}$$

The result of adding this numerical diffusion to the equations is shown in Fig. 2. After verification on a simple test problem (that of a circle with radius 0.25, Fig. 2a–d) allowing direct comparison of the numerical solution with the analytical solution, the parameter ε in Eqs. (4) and (6) was chosen to be equal to 10^{-4} for all the simulations in this study. If ε is too small, the numerical diffusion term in the smoothing procedure is negligible and oscillations appear in the calculation of the curvature leading to loss of smoothness in the definition of the interface (Fig. 2a). Contrarily, if ε is too high, excessive diffusion is added leading to a smooth but erroneous calculation of the curvature (Fig. 2c). Figure 2b shows the application of the smoothness on the calculation of the curvature distribution according to equation 4 on a 2D surface showing oscillations for too low levels of ε (Fig. 2e) and a smooth definition of the curvature for the proposed level of ε (Fig. 2f).

Once $\boldsymbol{n}$ and κ are computed, the advection velocity $\boldsymbol{u}$ is updated and Eq. (1) is solved. It is well known that this kind of equation (pure convection) solved with the finite element method leads to oscillations. To avoid this oscillatory behavior, the addition of a stabilization term (under many different forms) has been frequently described in the literature (Bochev et al. 2004). The drawback of this method is its

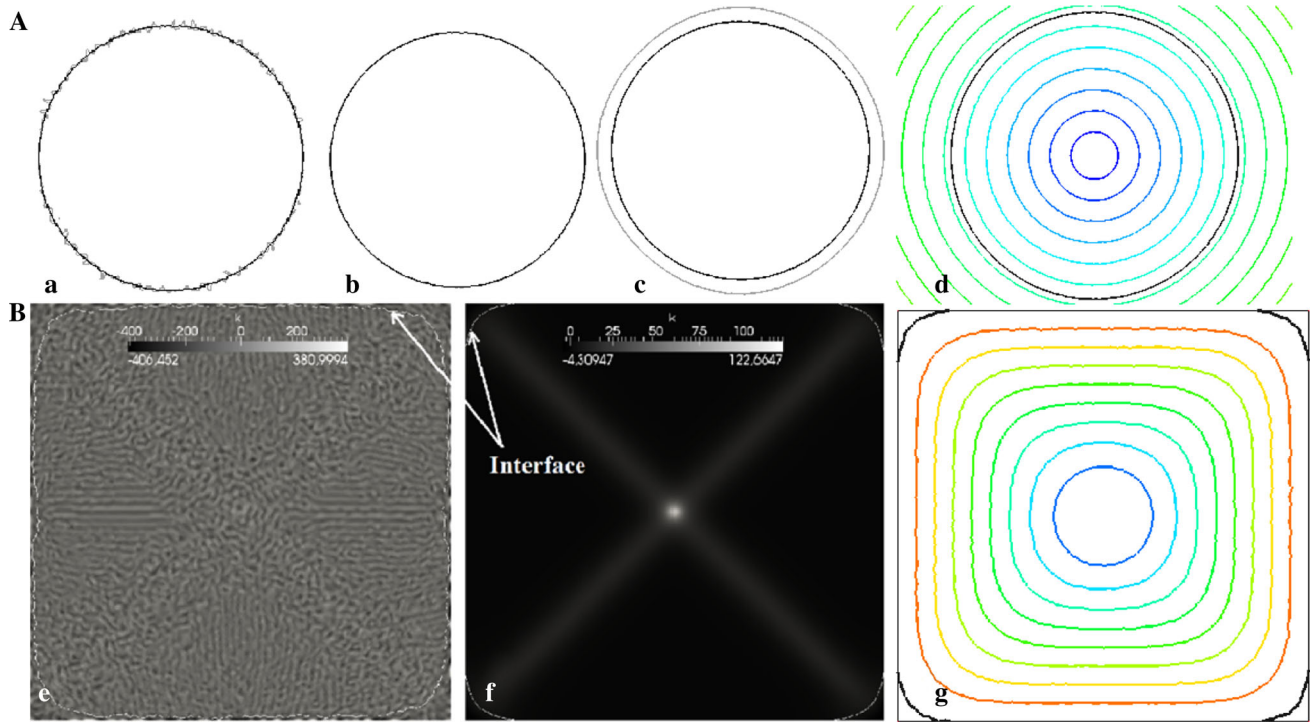

Fig. 2 Effect of adding numerical diffusion in the calculation of the curvature. **A** Comparison between analytic solution of curvature (1/radius) (in *black*) and numerical solution (in *gray*) for the curvature of a circle function of radius 0.25 in the unit square (*d*) for (*a*) $\varepsilon = 10^{-6}$, (*b*) $\varepsilon = 10^{-4}$, (*c*) $\varepsilon = 10^{-2}$, **B** calculation of the curvature κ of a distance function in the square (*black*: small curvature; *white*: high curvature). The interface ($\varphi = 0$) is represented with a *white line*. In (*e*), no numerical diffusion was added during the calculations so oscillations appear and the interface is not smooth. In (*f*), the curvature is correctly smoothed by diffusion and the interface is smooth due to the addition of a limited amount of numerical diffusion in the calculations. (*g*) Represent the iso-levels of the φ function (with in *thick black*, the interface)

computational cost. A cost efficient computational approach, implemented in FreeFem++, is the method of characteristics (Polyanin ADZ and Moussiaux 2002). This method consists of reducing a PDE to a system of ordinary differential equations (ODEs) along curves called 'characteristics'; the resolution of these ODEs along those curves leads to the solution of the original PDE. Given the explicit nature of the time integration scheme used in this study, the time step was fixed at 10^{-4} in a convergence study.

2.3 Experimental data

In this study, results presented in Van Bael et al. (2012) were used in a first calibration and validation round. The setup of the experiment is briefly repeated below. Six distinct unit cells were used which can be classified according to their shape as triangular, hexagonal and square, and according to their pore size. The pore sizes (measured in a 2D horizontal plane, cf Fig. 3(1) first row) used in this study were 500 and 1,000 μm (Fig. 3). The outer dimensions of the scaffold were 6 mm height and 6 mm diameter. Scaffolds were produced by a non-commercial, in-house-developed selective laser melting machine using Ti6Al4V powder (Raymor Industries Inc., Canada) as described in Van Bael et al. (2012). Each scaffold was drop seeded with 200,000 human periosteum-derived cells (hPDCs) (passage 5, additional details on the cell source can be found in Bari et al. (2006)) in 60 μl cell suspension and incubated statically for 1 h at 37° C to facilitate cell attachment, before being transferred to a rotator to perform dynamic rotation seeding. Cell seeding efficiencies between 80 and 95 % with significantly higher amounts of cells present on the small pore scaffolds which have the largest surface area (see Van Bael et al. 2012 for extensive discussion). After 6 h, the cell-seeded scaffolds were transferred to a 48-well plate and cultured in GM for 14 days. Medium was refreshed thrice a week. Cell growth on scaffolds was evaluated using the Live-Dead® viability/cytotoxicity staining (Invitrogen, USA) performed according to the provider's instructions. Homogeneous cell growth over the whole 3D surface was observed. Pictures of the growing cell/ECM domain (top and bottom of scaffold) were taken for 7 and 14 days of culture.

2.4 Objectives of this study

The aim of this study is to develop a computational framework that will enable modeling of the cell/ECM growth in

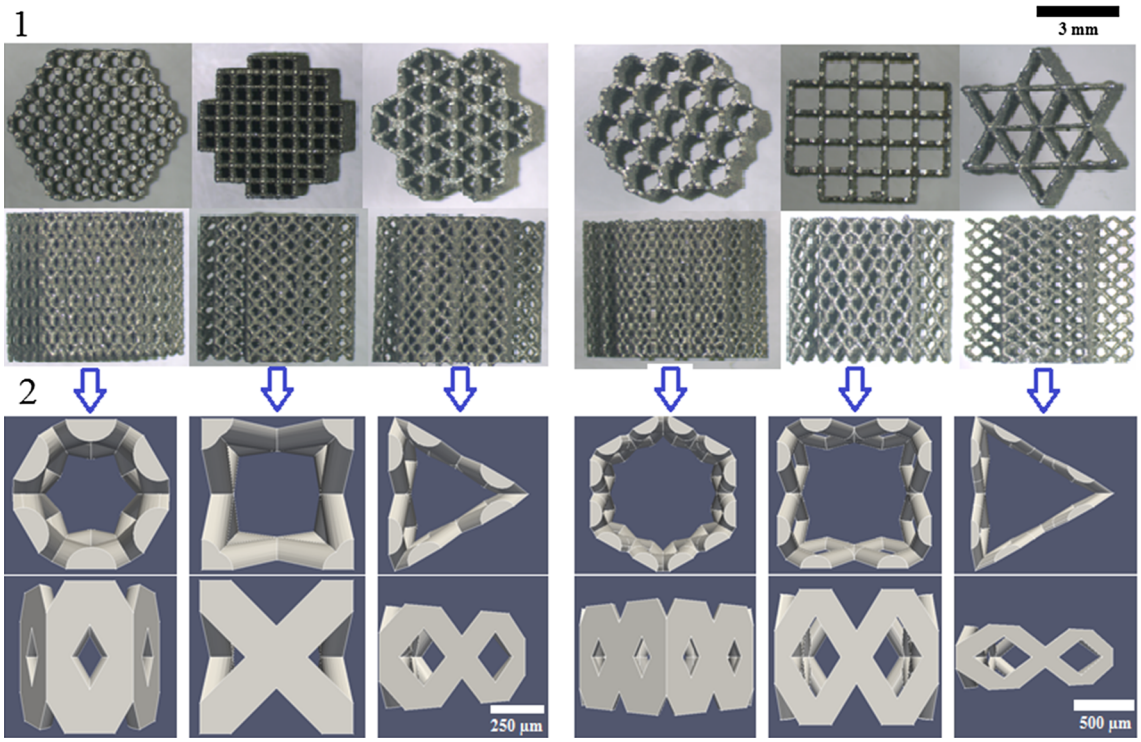

Fig. 3 (**1**) Different scaffold geometries (*hexagon*, *square*, and *triangle*) used in this study for pore size equal to 500 µm (*left*) and 1 mm (*right*). (**2**) Corresponding single pore for numerical simulations

porous structures. In this study, porous structures with various pore geometries and sizes were used. Cell seeding on these porous structures was represented by the initial condition in which the geometries were 'seeded' with a 10 µm thin layer of cell/ECM on the struts (Fig. 4). As the small pore scaffolds had the highest surface area and showed the highest cell seeding efficiencies, this simple initial condition reflected the observed experimental situation (Van Bael et al. 2012). For computational cost and accuracy, the simulation was performed on a single scaffold pore. Due to the regular geometry of the scaffolds used in this study, this simplification does not limit the generalization of the model predictions. Results are shown either for the entire pore or for half a pore in order to be able to investigate cell/ECM evolution within the pore.

Given the current absence of biological mechanistic details in the definition of the parameters describing cell/ECM growth, a calibration procedure was carried out based on experimental in vitro data to obtain a first assessment of the quantitative capabilities of the developed framework. Calibration of the model consisted of linking the simulation time (described by the number of iterations t using the fixed computational time step) to absolute time (days in culture). The parameter used for least square fitting was defined as the ratio of the 2D projected void pore surface, S_v (white part in Fig. 1) before and after cell culture (determined for both simulations and experiments). For the calculation of projected void pore surface from the experimental results, an average value was determined over 6 pores. First, the simulation time t (in this study, t is non-dimensional) needed to reach the projected void pore surface ratio equal to that of the experimentally measured one at culture day 7 was determined by best least square fitting for the hexagonal geometry. Subsequently, $t*2$ was used to predict S_v values at day 14 for all geometries.

3 Results

The in vitro experimental results were used to compare and calibrate the models (Fig. 6). Values of 'projected tissue area' (as a percentage of initial void area) obtained from live/dead images of the in vitro constructs provided 2D information regarding the development of cell/ECM construct in a static 3D culture over time. The comparison between in silico and in vitro results demonstrated a satisfying qualitative agreement in terms of shape. By least square fits a single calibration parameter (relating simulated time to experimental time) for all geometries of a same pore size was determined and led to good results. For the small pore size, $t = 1{,}500$ iterations corresponded to 7 days and $t = 3{,}000$ to 14 days of culture (Fig. 5a), while for the large pore size, $t = 7{,}000$ iterations corresponded to 7 days and $t = 14{,}000$ iterations to 14 days of culture (Fig. 5b). A quantitative evaluation of the projected tissue areas (both for computational and exper-

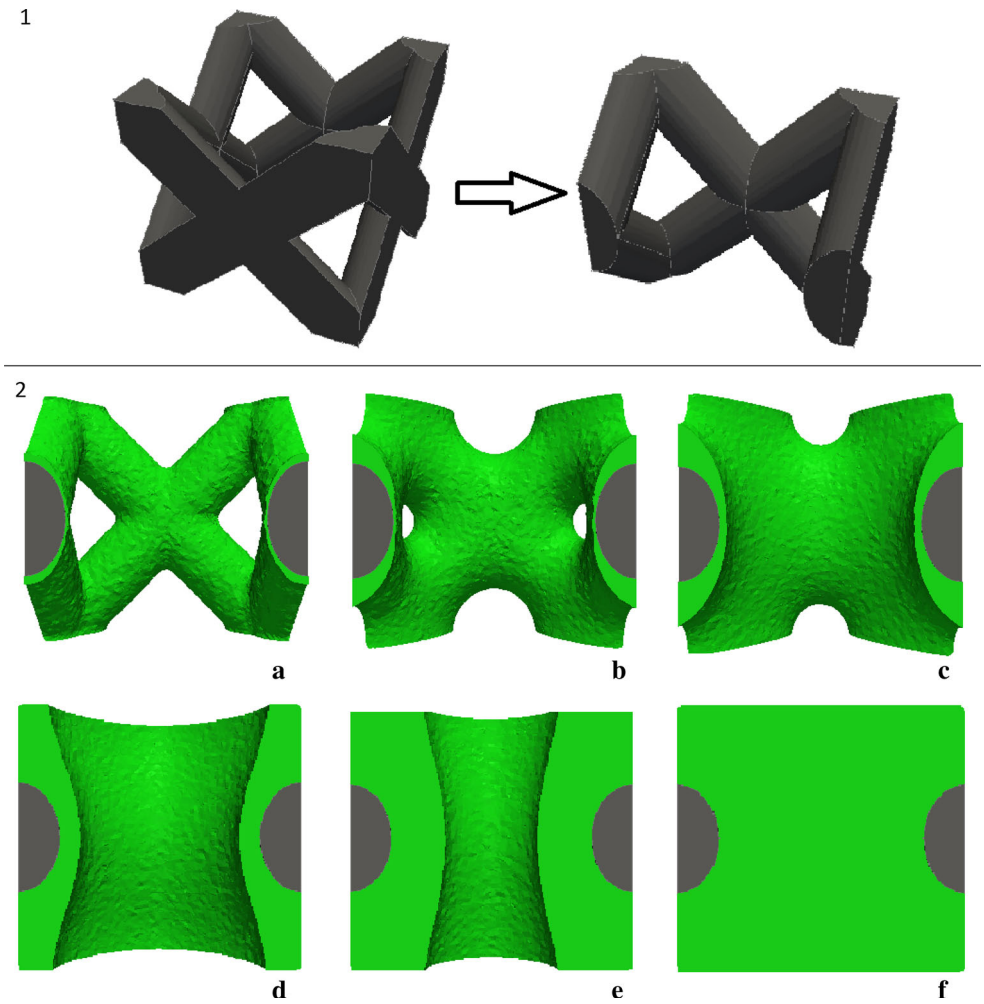

Fig. 4 (**1**) Pore geometry (*left*) an cut in half (*right*) for better visualization. (**2**) Cell/ECM growth (*green*) at (*a*) initial state, (*b*) 15 %, (*c*) 30 %, (*d*) 50 %, (*e*) 75 %, (*f*) 100 % of filling

imental results) of the aforementioned images is shown in Fig. 6a, b. The model predicts two successive stages during the cell/ECM growth process. The first one corresponds to the filling of the vertical small spaces between struts, and the second one is the filling of the pore itself. For instance, for the case of 1 mm pore size scaffolds, the hexagon presents very small vertical spaces leading to an acceleration of the cell/ECM growth at the very beginning, whereas for the triangle shaped scaffold, the vertical spaces were so large that they did not reach complete filling for the entire duration of the simulation, and therefore, the second growth stage could not be observed. A good correspondence between computational and experimental results was obtained where the simulated projected tissue area was systematically less than one standard deviation away from the experimentally observed mean projected tissue area. In more complex geometries, such as the one shown in Fig. 7, particular behavior such as bridging between different local surfaces during cell/ECM growth can be observed which is treated automatically with the LS method in contrast to other techniques that previously have been reported to implement curvature-dependent growth.

4 Discussion

This study provides a 'proof of concept' on the use of the LS computational method as a tool to investigate 3D cell/ECM growth on a range of titanium alloy (Ti6Al4V) scaffold architectures that are relevant to tissue engineering (TE) applications. The preference of cells to spontaneously grow in a 3D cell/ECM network structure rather than in a flattened 2D manner when cultured in vitro on 3D scaffolds has been reported in numerous studies (Papantoniou et al. 2013b; Knychala et al. 2013; Papantoniou et al. 2013a; Grayson et al. 2004). In this study, a range of pore geometries was studied. Initial results showed that the curvature-driven growth was correctly implemented capturing known qualitative features of cell/ECM growth. Irrespective of the initial pore

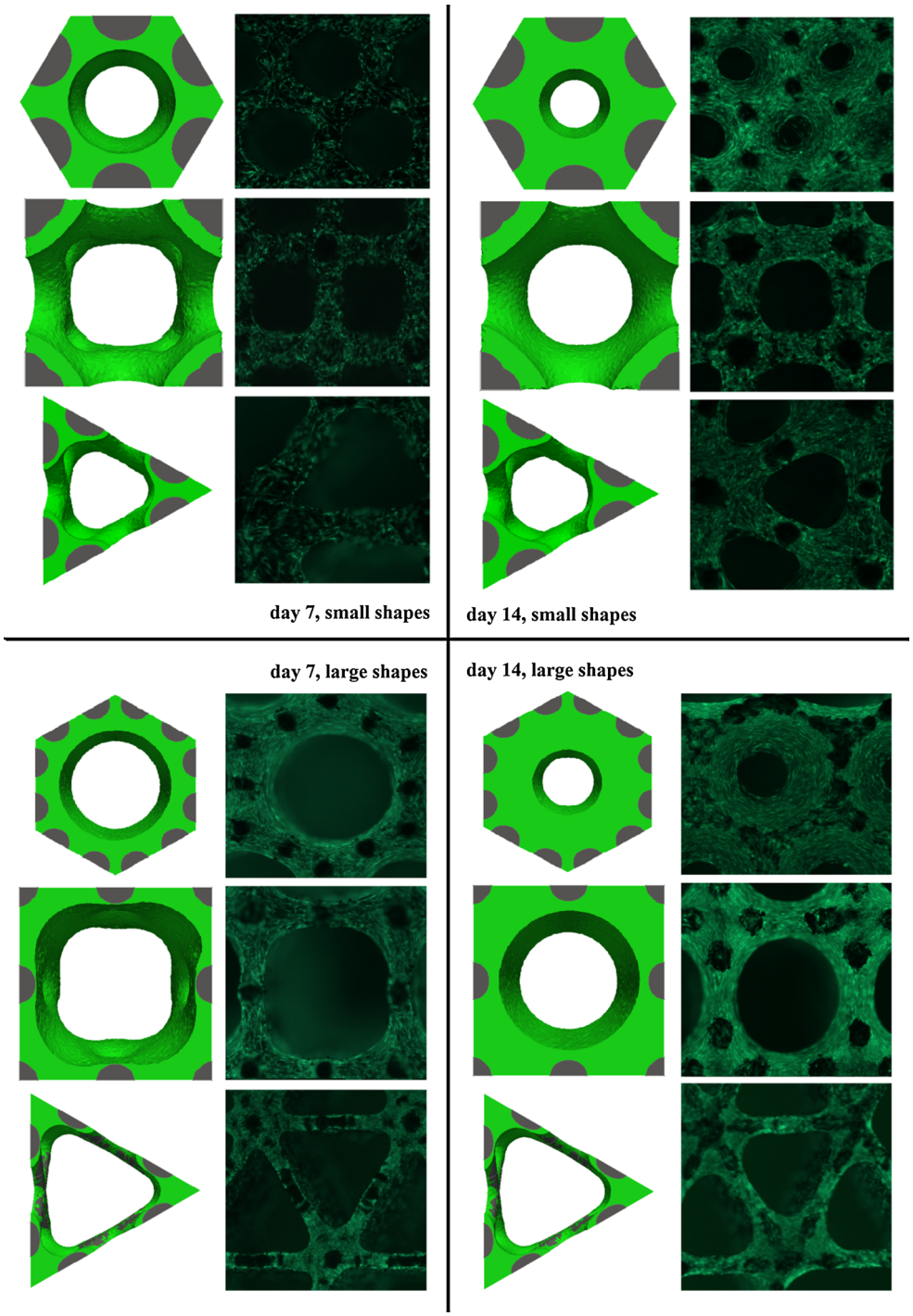

Fig. 5 Qualitative comparison between simulations and experiments. Numerical results are shown on the *white background*, experimental results (live-dead staining) are shown on the *black background* at day 7 (*left*) and day 14 (*right*) for the 0.5 mm (*top*) and 1 mm (*bottom*) scaffold geometries

shape (Kommareddy et al. 2010; Rumpler et al. 2008), all simulations eventually resulted in 'spherical' or 'cylindrical' geometries with positive curvatures at the corners leading to higher velocities of interface growth, as observed by others (Rumpler et al. 2008; Knychala et al. 2013) and negative curvatures at the middle of the struts. Hexagonal pore scaffolds possessing a shape that is closest to that of a circle showed a faster growth of the cell/ECM domain, while triangular pore scaffolds were seen to induce the slowest growth, in agreement with what has been observed in our experiments and reported in the literature to date (Rumpler et al. 2008; Knychala et al. 2013; Bidan et al. 2013a).

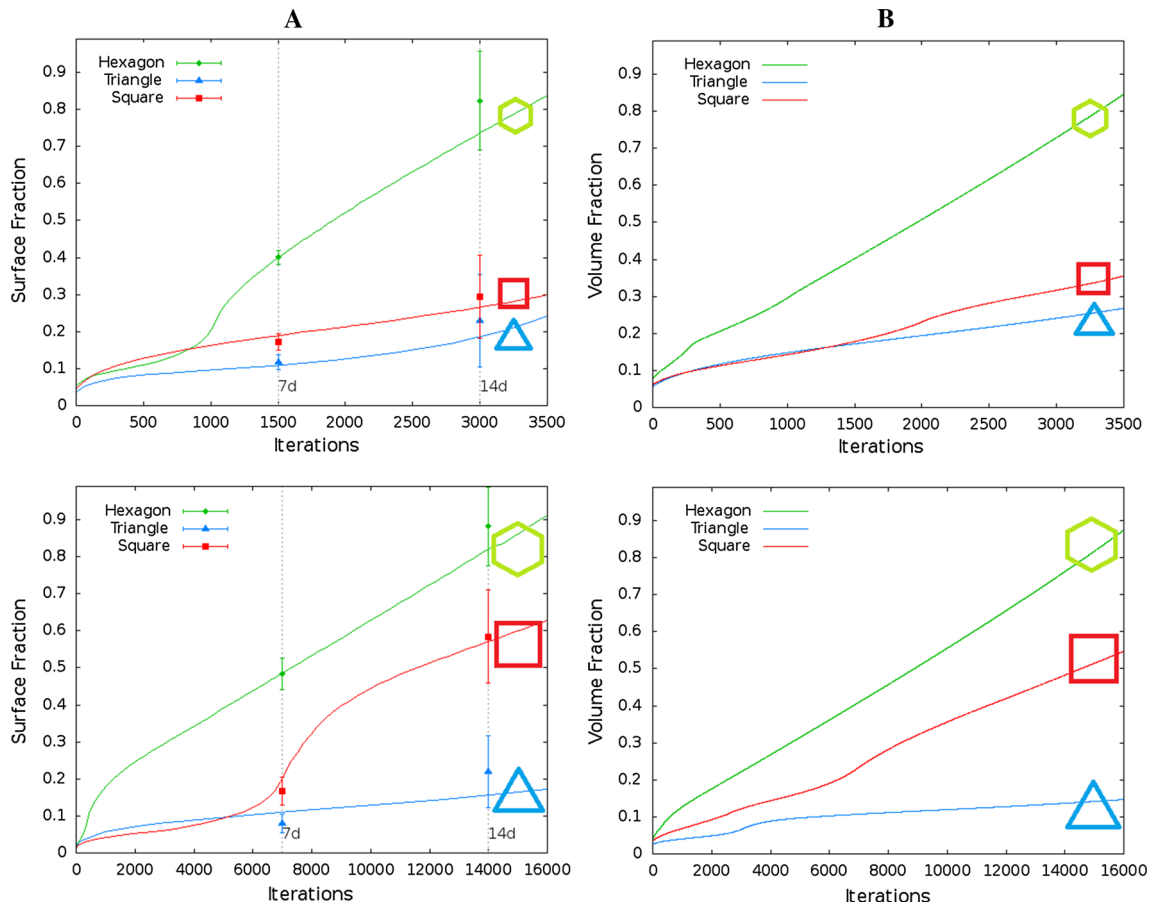

Fig. 6 **a** Quantitative comparison between simulations and experiments. Surface fraction from a cross section (*continuous line*) for 0.5 mm (*top*) and 1 mm (*bottom*) geometries versus experimental projected area (data points, average ± standard deviation for 6 pores). **b** Volume fraction (*continuous line*) for 0.5 mm (*top*) and 1 mm (*bottom*) geometries

The use of curvature-driven growth models has been shown to be an efficient approach when investigating biological constructs in 2D (Rumpler et al. 2008; Bidan et al. 2012; Knychala et al. 2013). However, due to the complexity of many scaffold geometries and a lack of symmetry (regarding the different axes), 2D approximations were employed limiting thus their predictive capabilities regarding cell/ECM distribution in 3D structures with realistic design features. This study proposed a 3D modeling approach able to interpret a local change in the curvature and to use it to guide the growth rate. Furthermore, it showed that the LS method is a powerful approach in the context of curvature-driven growth simulation due to its intrinsic evaluation of the direction of interface motion and curvature, reducing in this way user intervention. In previous studies in both 2D (Bidan et al. 2012) and 3D (Bidan et al. 2013b), a mask was used over a digital (pixelated) images to determine the local curvature of the construct and use it to update the interface. This approach, although allowing for easy implementation of novel geometries due to the explicit use of CT data as input, requires substantial input by the user when choosing an efficient mask size. Additionally, upscaling to 3D was not straightforward, especially when dealing with complex pore structures, combining larger and smaller curvatures. In this study, the user intervention was strongly reduced due to the model's ability to determine the local curvature; the only intervention required is that of setting the initial mesh size of the pore. This study shows the potential of the LS approach in capturing curvature-driven cell/ECM growth on different geometries including complex, irregular, and non-symmetric shapes. Due to the very nature of the LS method and its ability to treat changes in topology, this model was able to simulate particular behavior such as bridging between two local surfaces when moving in the same direction (Fig. 7).

Despite the advantages inherent to the use of the LS method for simulating cell/ECM growth, the model in its current form faces a number of limitations. Indeed, even though user intervention was minimized, a mesh of the pore domain still has to be constructed. The mesh size has to be of sufficient quality, as an overly coarse mesh could lead to incorrect results. Additionally, during the calibration phase, a factor 5 difference in the ratio experimental time versus

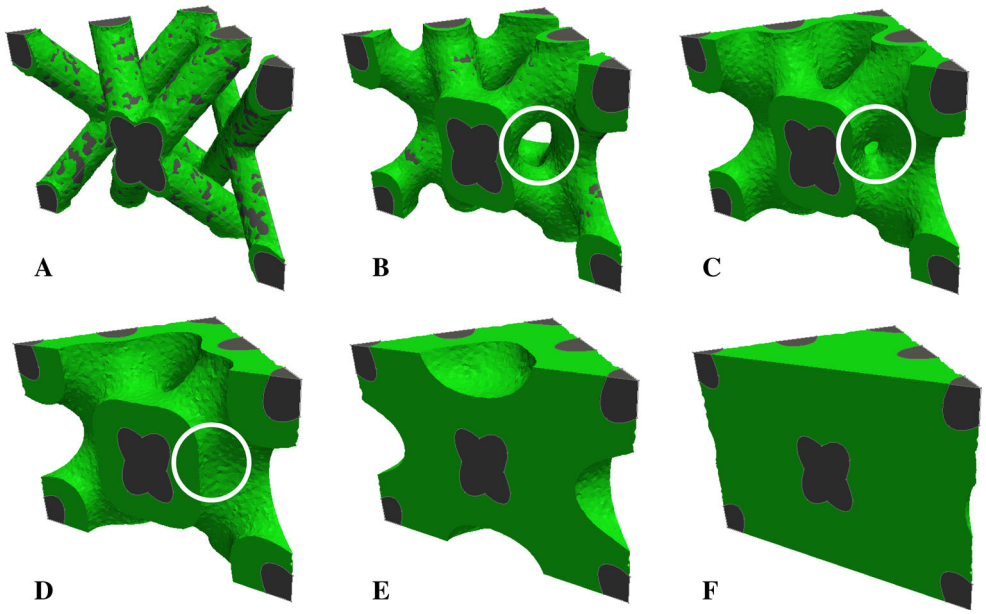

Fig. 7 Cell/ECM growth on a complex geometry with diamond shaped pores. Results are shown for different degrees of pore filling: 8 % (**a**), 15 % (**b**), 30 % (**c**), 50 % (**d**), 75 % (**e**), and 98 % (**f**) . The pore has being cut in half (diagonally) for a better visualization of the simulated growth. These results illustrate the bridging process (*white circle*) and the subsequent change in topology when two local surfaces move in the same direction

simulation time was found between geometries with 1 mm versus 500 μm pore size. This means that in the experiments, absolute cell/ECM growth was observed to be 5 times faster in the larger pores compared to the smaller pores. When incorporating this experimentally observed difference in growth velocity in the simulations (multiplying the right-hand side of equation 3 by a factor 5 for the large pores), the ratio experimental time versus simulation time becomes the same for both pore sizes. The difference in experimental growth speed could be caused by various factors, among which the limitation of nutrient supply in the case of smaller pores (on the inside of the scaffold) and is the subject of ongoing investigations. This means that although the parameters defining the growth rate for various geometries with a similar pore size are equal, these parameters need to be altered when larger pore sizes are modeled. Currently, the growth rate only depends on the local curvature, adding additional biological insights (related to e.g., the effect of mass transport on cell/ECM growth) in combination with additional structural parameters (e.g., available surface area) might provide a solution.

Potentially, the introduction of other influencing factors in Eq. (1) such as mass transport, oxygen consumption, and medium composition could help to explain the difference in calibration factor between geometries with small and large pore sizes. The introduction of space- and time-dependent parameters representing the biology in a more mechanistic way will be the subject of future work. When considering mass transport in the model, a coupling with fluid dynamics also needs to be established. The level set method has already been successfully used in conjunction with fluid dynamic and oxygen and nutrient consumption models in the simulation of cartilage growth in an in vitro culture system (Lappa 2005, 2003b), whereas the model by Lappa (35) was limited to 2D, the multiphysics approach of combining curvature-dependent growth with fluid dynamics could be extended to the third dimension. Finally, the quantitative calibration/validation carried out in this study was based on '2D projected void areas' which constitutes a considerable simplification since both computational and experimental results were obtained in 3D settings. In order to overcome this limitation, it is necessary to develop and use more realistic and information-rich validation techniques. The use of computer tomography techniques such as microCT, nanoCT, and CE-nanoCT to analyze and monitor 3D cell/ECM growth (Voronov et al. 2012; Lenthe et al. 2007; Papantoniou et al. 2013a) on complex geometries could offer substantial improvement to the model by allowing for a more accurate validation of cell/ECM growth kinetics and is something that will be further pursued.

The results obtained by this study provide crucial feedback that would allow the intelligent design of (3D porous) TE scaffolds that may actively guide 3D cell growth and final cell/ECM construct characteristics. Based on the presented computational tool, a wide range of biologically relevant 3D scaffold designs could be tested in silico prior to the manufacturing phase. Furthermore, given the additional complexities introduced by the use of dynamic culture conditions,

i.e., in bioreactor setups, a multiphysics model could pose as an attractive platform for further integrated studies on the interplay between scaffold design features and process conditions and their decoupled and combined effect on cell/ECM growth.

In this study, we developed an LS-based computational framework to predict the final shape of a biological construct in static culture conditions for a given scaffold geometry. Various geometries and pore sizes were examined both experimentally and numerically, and a good qualitative and quantitative behavior of the framework was demonstrated. The model in its current form is able to provide important information on the shape and the speed of the filling of tissue-engineered constructs by cells and ECM.

Acknowledgments Y.G. is funded by Belgian National Fund for Scientific Research (FNRS) grant FRFC 2.4564.12. I.P. is funded by the ENDEAVOUR project G.0982.11N of the Research Foundation Flanders (FWO Vlaanderen). The research leading to these results has received funding from the European Research Council under the European Union's Seventh Framework Programme (FP/2007-2013)/ERC Grant Agreement No. 279100. This work is part of Prometheus, the Leuven R&D division of Skeletal Tissue Engineering.

References

AlMomani T, Udaykumar HS, Marshall JS, Chandran KB (2008) Micro-scale dynamic simulation of erythrocyte–platelet interaction in blood flow. Ann Biomed Eng 36(6):905–920. doi:10.1007/s10439-008-9478-z

Bidan CM, Kommareddy KP, Rumpler M, Kollmannsberger P, Brechet YJM, Fratzl P, Dunlop JWC (2012) How linear tension converts to curvature: geometric control of bone tissue growth. PloS One 7(5). doi:10.1371/journal.pone.0036336

Bidan CM, Kommareddy KP, Rumpler M, Kollmannsberger P, Fratzl P, Dunlop JW (2013a) Geometry as a factor for tissue growth: towards shape optimization of tissue engineering scaffolds. Adv Healthc Mater 2(1):186–194. doi:10.1002/adhm.201200159

Bidan CM, Wang FM, Dunlop JW (2013) A three-dimensional model for tissue deposition on complex surfaces. Comput Methods Biomech Biomed Eng. doi:10.1080/10255842.2013.774384

Bochev PB, Gunzburger MD, Shadid JN (2004) Stability of the SUPG finite element method for transient advection-diffusion problems. Comput Method Appl Mech 193(23–26):2301–2323. doi:10.1016/j.cma.2004.01.026

Chai YC, Kerckhofs G, Roberts SJ, Van Bael S, Schepers E, Vleugels J, Luyten FP, Schrooten J (2012) Ectopic bone formation by 3D porous calcium phosphate-Ti6Al4V hybrids produced by perfusion electrodeposition. Biomaterials 33(16):4044–4058. doi:10.1016/j.biomaterials.2012.02.026

Chai YC, Roberts SJ, Van Bael S, Chen Y, Luyten FP, Schrooten J (2012b) Multi-level factorial analysis of Ca2+/Pi supplementation as bio-instructive media for in vitro biomimetic engineering of three-dimensional osteogenic hybrids. Tissue Eng Part C Methods 18(2):90–103. doi:10.1089/ten.TEC.2011.0248

De Bari C, Dell'Accio F, Vanlauwe J, Eyckmans J, Khan IM, Archer CW, Jones EA, McGonagle D, Mitsiadis TA, Pitzalis C, Luyten FP (2006) Mesenchymal multipotency of adult human periosteal cells demonstrated by single-cell lineage analysis. Arthr Rheum 54(4):1209–1221. doi:10.1002/art.21753

Dunlop JWC, Fischer FD, Gamsjager E, Fratzl P (2010) A theoretical model for tissue growth in confined geometries. J Mech Phys Solids 58(8):1073–1087. doi:10.1016/j.jmps.2010.04.008

Eyckmans J, Boudou T, Yu X, Chen CS (2011) A Hitchhiker's guide to mechanobiology. Dev Cell 21(1):35–47. doi:10.1016/j.devcel.2011.06.015

Gamsjager E, Bidan CM, Fischer FD, Fratzl P, Dunlop JW (2013) Modelling the role of surface stress on the kinetics of tissue growth in confined geometries. Acta Biomater 9(3):5531–5543. doi:10.1016/j.actbio.2012.10.020

Grayson WL, Ma T, Bunnell B (2004) Human mesenchymal stem cells tissue development in 3D PET matrices. Biotechnol Progr 20(3):905–912. doi:10.1021/bp034296z

Hecht F (2012) New development in freefem++. J Numer Math 20(3–4):251–265. doi:10.1515/jnum-2012-0013

Higuchi A, Ling QD, Chang Y, Hsu ST, Umezawa A (2013) Physical cues of biomaterials guide stem cell differentiation fate. Chem Rev 113(5):3297–3328. doi:10.1021/cr300426x

Hogea CS, Murray BT, Sethian JA (2006) Simulating complex tumor dynamics from avascular to vascular growth using a general level-set method. J Math Biol 53(1):86–134. doi:10.1007/s00285-006-0378-2

Hollister SJ, Maddox RD, Taboas JM (2002) Optimal design and fabrication of scaffolds to mimic tissue properties and satisfy biological constraints. Biomaterials 23(20):4095–4103

Javierre E, Vuik C, Vermolen F, Segal A, van der Zwaag S (2006) The level set method for solid-solid phase transformations. Numer Math Adv Appl 712–719. doi:10.1007/978-3-540-34288-5_69

Knychala J, Bouropoulos N, Catt CJ, Katsamenis OL, Please CP, Sengers BG (2013) Pore geometry regulates early stage human bone marrow cell tissue formation and organisation. Ann Biomed Eng 41(5):917–930. doi:10.1007/s10439-013-0748-z

Kommareddy KP, Lange C, Rumpler M, Dunlop JWC, Manjubala I, Cui J, Kratz K, Lendlein A, Fratzl P (2010) Two stages in three-dimensional in vitro growth of tissue generated by osteoblastlike cells. Biointerphases 5(2):45–52. doi:10.1116/1.3431524

Lappa M (2003a) The growth and the fluid dynamics of protein crystals and soft organic tissues: models and simulations, similarities and differences. J Theor Biol 224(2):225–240. doi:10.1016/S0022-5193(03)00160-7

Lappa M (2003b) Organic tissues in rotating bioreactors: fluid-mechanical aspects, dynamic growth models, and morphological evolution. Biotechnol Bioeng 84(5):518–532. doi:10.1002/bit.10821

Lappa M (2005) A CFD level-set method for soft tissue growth: theory and fundamental equations. J Biomech 38(1):185–190. doi:10.1016/j.jbiomech.2004.02.037

Lutolf MP, Hubbell JA (2005) Synthetic biomaterials as instructive extracellular microenvironments for morphogenesis in tissue engineering. Nat Biotechnol 23(1):47–55. doi:10.1038/nbt1055

Machacek M, Danuser G (2006) Morphodynamic profiling of protrusion phenotypes. Biophys J 90(4):1439–1452. doi:10.1529/biophysj.105.070383

Melchels FP, Barradas AM, van Blitterswijk CA, de Boer J, Feijen J, Grijpma DW (2010) Effects of the architecture of tissue engineering scaffolds on cell seeding and culturing. Acta Biomater 6(11):4208–4217

Melchels FP, Tonnarelli B, Olivares AL, Martin I, Lacroix D, Feijen J, Wendt DJ, Grijpma DW (2011) The influence of the scaffold design on the distribution of adhering cells after perfusion cell seeding. Biomaterials 32(11):2878–2884. doi:10.1016/j.biomaterials.2011.01.023

Nelson CM, Jean RP, Tan JL, Liu WF, Sniadecki NJ, Spector AA, Chen CS (2005) Emergent patterns of growth controlled by multicellular form and mechanics. Proc Natl Acad Sci USA 102(33):11594–11599. doi:10.1073/pnas.0502575102

Papantoniou I, Sonnaert M, Geris L, Luyten FP, Schrooten J, Kerckhofs G (2013a) Three dimensional characterization of tissue-engineered constructs by contrast enhanced nanofocus computed tomography. Tissue Eng Part C Methods. doi:10.1089/ten.TEC.2013.0041

Papantoniou II, Chai YC, Luyten FP, Schrooten JI (2013b) Process quality engineering for bioreactor-driven manufacturing of tissue-engineered constructs for bone regeneration. Tissue Eng Part C Methods. doi:10.1089/ten.TEC.2012.0526

Polyanin ADZ VF, Moussiaux A (2002) Handbook of first order partial differential equations. Taylor & Francis, London

Rumpler M, Woesz A, Dunlop JWC, van Dongen JT, Fratzl P (2008) The effect of geometry on three-dimensional tissue growth. J R Soc Interface 5(27):1173–1180. doi:10.1098/rsif.2008.0064

Sethian JA (1999) Fast marching methods. Siam Rev 41(2):199–235. doi:10.1137/S0036144598347059

Shraiman BI (2005) Mechanical feedback as a possible regulator of tissue growth. Proc Natl Acad Sci USA 102(9):3318–3323. doi:10.1073/pnas.0404782102

Sobral JM, Caridade SG, Sousa RA, Mano JF, Reis RL (2011) Three-dimensional plotted scaffolds with controlled pore size gradients: effect of scaffold geometry on mechanical performance and cell seeding efficiency. Acta Biomater 7(3):1009–1018. doi:10.1016/j.actbio.2010.11.003

Van Bael S, Chai YC, Truscello S, Moesen M, Kerckhofs G, Van Oosterwyck H, Kruth IP, Schrooten J (2012) The effect of pore geometry on the in vitro biological behavior of human periosteum-derived cells seeded on selective laser-melted Ti6Al4V bone scaffolds. Acta Biomater 8(7):2824–2834. doi:10.1016/j.actbio.2012.04.001

Van Bael S, Chai YC, Truscello S, Moesen M, Kerckhofs G, Van Oosterwyck H, Kruth JP, Schrooten J (2012) The effect of pore geometry on the in vitro biological behavior of human periosteum-derived cells seeded on selective laser-melted Ti6Al4V bone scaffolds. Acta Biomater 8(7):2824–2834. doi:10.1016/j.actbio.2012.04.001

Van Bael S, Kerckhofs G, Moesen M, Pyka G, Schrooten J, Kruth JP (2011) Micro-CT-based improvement of geometrical and mechanical controllability of selective laser melted Ti6Al4V porous structures. Mater Sci Eng A Struct 528(24):7423–7431. doi:10.1016/j.msea.2011.06.045

van Lenthe GH, Hagenmuller H, Bohner M, Hollister SJ, Meinel L, Muller R (2007) Nondestructive micro-computed tomography for biological imaging and quantification of scaffold-bone interaction in vivo. Biomaterials 28(15):2479–2490

Voronov RS, Vangordon SB, Shambaugh RL, Papavassiliou DV, Sikavitsas VI (2012) 3D Tissue engineered construct analysis via conventional high resolution MicroCT without X-ray contrast. Tissue Eng Part C Methods. doi:10.1089/ten.TEC.2011.0612

Zeltinger J, Landeen LK, Alexander HG, Kidd ID, Sibanda B (2001a) Development and characterization of tissue-engineered aortic valves. Tissue Eng 7(1):9–22. doi:10.1089/107632701300003250

Zeltinger J, Sherwood JK, Graham DA, Mueller R, Griffith LG (2001b) Effect of pore size and void fraction on cellular adhesion, proliferation, and matrix deposition. Tissue Eng 7(5):557–572. doi:10.1089/107632701753213183